ACS APPLIED MATERIALS & INTERFACES

www.acsami.org Research Article

Self-Limiting Opto-Electrochemical Thinning of Transition-Metal Dichalcogenides

Suichu Huang, Jingang Li, Jie Fang, Hongru Ding, Wentao Huang, Xuezeng Zhao,* and Yuebing Zheng*

Cite This: *ACS Appl. Mater. Interfaces* 2021, 13, 58966−58973 Read Online

ACCESS | Metrics & More | Article Recommendations | Supporting Information

ABSTRACT: Two-dimensional monolayer and few-layer transition-metal dichalcogenides (TMDs) are promising for advanced electronic and photonic applications due to their extraordinary optoelectronic and mechanical properties. However, it has remained challenging to produce high-quality TMD thin films with controlled thickness and desired micropatterns, which are essential for their practical implementation in functional devices. In this work, a self-limiting opto-electrochemical thinning (sOET) technique is developed for on-demand thinning and patterning of TMD flakes at high efficiency. Benefiting from optically enhanced electrochemical reactions, sOET features a low operational optical power density of down to 70 $\mu W\ \mu m^{-2}$ to avoid photodamage and thermal damage to the thinned TMD flakes. Through selective optical excitation with different laser wavelengths based on the thickness-dependent band gaps of TMD materials, sOET enables precise control over the final thickness of TMD flakes. With the capability of thickness control and site-specific patterning, our sOET offers an effective route to fabricating high-quality TMD materials for a broad range of applications in nanoelectronics, nanomechanics, and nanophotonics.

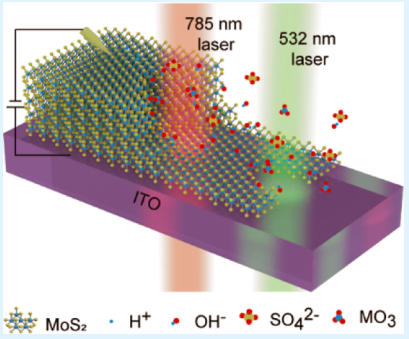

KEYWORDS: *laser thinning, transition-metal dichalcogenides, opto-electrochemical, self-limiting, layer-dependent*

INTRODUCTION

Since the discovery of graphene,[1] atomically thin two-dimensional (2D) materials have attracted great interest, owing to their extraordinary properties, such as large surface-to-volume ratio, large exciton binding energies, and valley-dependent photonics and optoelectronics.[2−11] Unlike zero-band gap graphene,[12] monolayers of transition-metal dichalcogenides (TMDs), such as MoS_2, WS_2, and WSe_2, exhibit a direct band gap ranging from visible to near-infrared light frequency.[5] Besides monolayers, few-layer TMDs also present unique and intriguing phenomena, such as interlayer excitons,[13,14] piezoelectricity,[15] and superconductivity.[16,17] Additionally, 2D TMDs possess other excellent features, including large surface-to-volume ratio, strong spin−orbit coupling, and spin-valley locking, making them promising for many applications in photodetection,[18−20] valleytronics,[21,22] sensing,[23,24] biomedical imaging,[25,26] and drug delivery.[27−29]

To fully unleash the potential of TMD materials, it is essential to fabricate high-quality TMD flakes with controlled thickness and microstructures. Mechanical exfoliation is widely exploited to prepare high-quality monolayer and few-layer TMD flakes. However, mechanically exfoliated TMD flakes are usually in small lateral sizes and with poor thickness control.[30,31] In contrast, the liquid-phase exfoliation method is more scalable, but it may result in poor quality and unwanted contaminations.[32−34] Alternatively, synthetic approaches, such as chemical vapor deposition (CVD) and molecular beam epitaxy (MBE), can produce TMD monolayers on a large scale.[35,36] However, both CVD and MBE require complex and expensive equipment, and the electrical properties of the chemically grown TMDs are typically inferior to the exfoliated ones.

Recently, laser thinning has emerged as a promising top-down approach for low-cost and high-throughput fabrication of TMD layers with site-specific control.[37] For instance, on-demand thinning of MoS_2 with layer-by-layer precision was demonstrated with a high-fluence laser beam (30−80 mW m^{-2}) to burn the top layers.[38] Yet, this high optical power leads to a notable temperature increase, which could induce the phase transition of TMDs and affect the quality of the thinned films.[39] In another approach, Nagareddy et al. demonstrated on-demand thinning of $MoTe_2$ flakes by a much lower laser fluence (0.3−4 mW m^{-2}) with the assistance of adsorbed water vapor on the flake surface.[40] However, this thinning process relies on the weak thermal and chemical stability of $MoTe_2$,[41] which is not applicable to other TMD materials with strong interatomic bonding, such as MoS_2 and WS_2.

Alternatively, optoelectronic thinning has been proposed to realize the thinning of TMDs in aqueous solutions through

Received: October 5, 2021
Accepted: November 19, 2021
Published: December 1, 2021

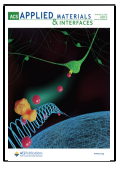

https://doi.org/10.1021/acsami.1c19163
ACS Appl. Mater. Interfaces 2021, 13, 58966−58973

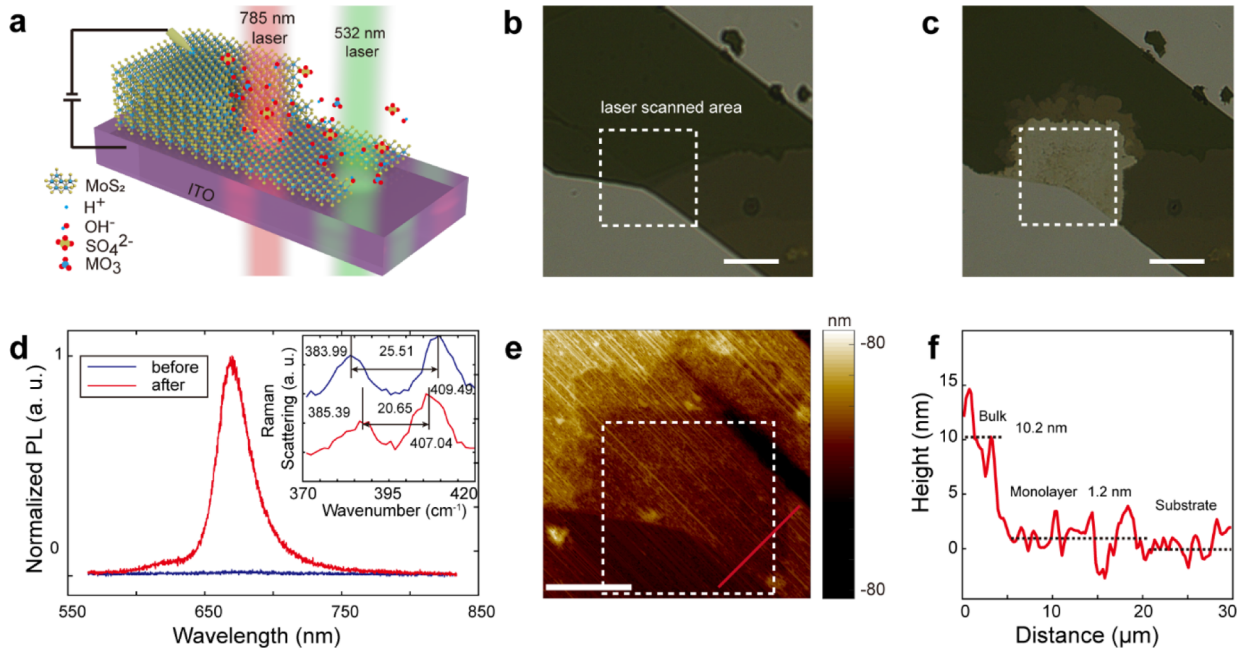

Figure 1. General concept of sOET. (a) Schematic of sOET. A 785 nm laser leads to the thinning of a thick MoS_2 flake to monolayers, while a 532 nm laser removes all the flakes. (b) Optical image of a thick MoS_2 flake on ITO before thinning. (c) Same flake in (b) after being partially thinned by a 785 nm laser. The laser scanned area is indicated by the white dashed square. (d) PL spectra of the flake before (blue) and after (red) thinning. The inset shows the Raman scattering spectra before (blue) and after (red) thinning. (e) AFM image of the thinned flake. (f) AFM height profile of the red line in (e) from top right to bottom left. All scale bars are 20 μm.

optically controlled electrochemical etching. In comparison to direct laser thinning via thermal sublimation, the electrochemical approaches typically require a much lower temperature, which enables the removal of top layers without sacrificing properties of the bottom layer.[42] Optoelectronic thinning of bulk MoS_2 was demonstrated to prepare monolayers on gold substrates.[43,44] However, the reliable production of the monolayer MoS_2 was challenging due to the reliance on the electrochemical reaction time, which would demand high-resolution *in situ* monitoring of the number of the layers and an effective method to terminate the reaction once the monolayer is achieved. In addition, the capability to precisely control the final thickness of the thinned TMD flakes in a layer-by-layer fashion has remained elusive. Such a precise control is critical to applications that require an exact number of layers (i.e., one, two, or more layers).

Herein, we report a self-limiting opto-electrochemical thinning (sOET) technique for on-demand thinning and patterning of TMDs. The optically activated electrochemical etching automatically stops once TMD flakes are thinned to the targeted thicknesses (i.e., one, two or more layers), which is accomplished by using the specific laser wavelength depending on the band gap energy of the targeted number of layers. No sophisticated engineering of thinning conditions is needed. We further demonstrate the high-throughput thinning of large TMD flakes down to the monolayer with equivalent quality to pristine exfoliated monolayers. Together with the low-power operation, general applicability, and tunable thinning rates, our sOET provides new possibilities in the reliable fabrication of high-quality TMDs for their applications in advanced electronic and photonic devices.

RESULTS AND DISCUSSION

Basic Concepts of sOET. The general concept of sOET is shown in Figure 1a. Briefly, a thick TMD flake, such as MoS_2, is transferred onto an indium tin oxide (ITO) substrate. Meanwhile, the flake is immersed in deionized (DI) water and biased with a suspending electrode in the liquid (see Figure S1 for experimental setup, Supporting Information). To enable the light-directed electrochemical thinning of MoS_2, we direct a laser beam onto the flake to excite electrons from the valence band to the conduct band and generate electron−hole pairs. Under an electrical bias, electrons are conducted to the suspending electrode, leaving excessive holes in the flake. At the edge or defect of the flake, MoS_2 can be oxidized in the presence of holes and hydroxide ions via the electrochemical reactions[44,45]

$$MoS_2 + OH^- + h^+ \rightarrow MoS_3 + SO_4^{2-} + H_2O \quad (1)$$

As a proof-of-concept demonstration, we show the laser thinning of a pristine thick MoS_2 flake prepared by mechanical exfoliation (Figure 1b). After being illuminated by a 785 nm laser with a power density of 69.6 $\mu W\ \mu m^{-2}$ under 0.2 V bias, the scanned area was successfully thinned (Figure 1c). The atomic force microscopy (AFM) measurement reveals that the flake was thinned from ~10.2 to ~1.2 nm, which indicates a monolayer (Figure 1e,f). After laser scanning, the as-thinned region showed dramatically enhanced photoluminescence (PL) at 673 nm (Figure 1d), confirming its monolayer feature. In addition, the difference between E^1_{2g} and A_{1g} Raman modes was reduced from ~25.5 to ~20.6 cm^{-1} (inset in Figure 1d, also see Figure S3 for spatial mapping of Raman scattering and PL signals, Supporting Information), which agrees well with the Raman spectra of the monolayer MoS_2.[46,47] This opto-electrochemical thinning will not affect the quality of the thinned monolayer, which is highly stable and shows no

https://doi.org/10.1021/acsami.1c19163
ACS Appl. Mater. Interfaces 2021, 13, 58966−58973

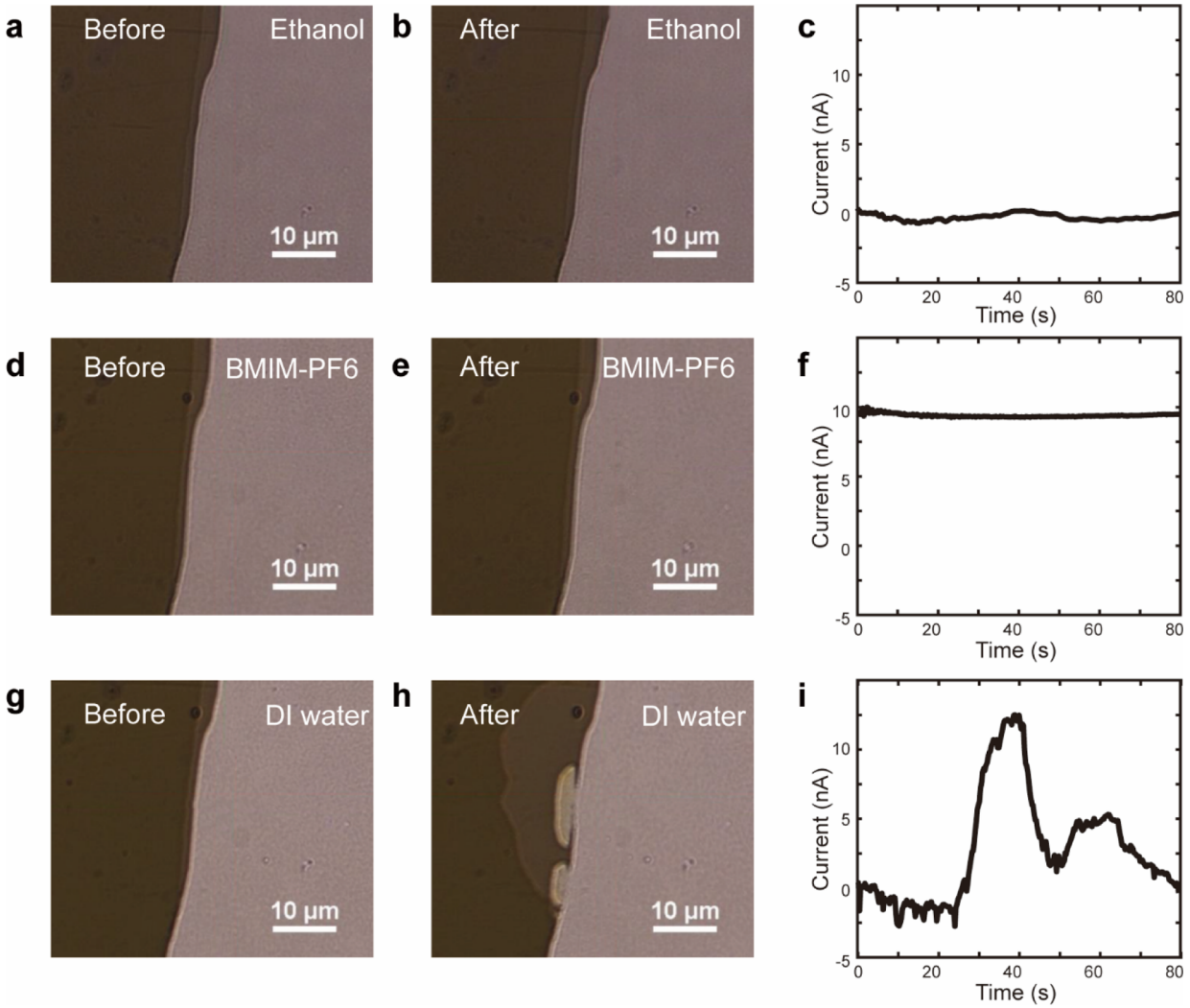

Figure 2. Opto-electrochemical thinning in different solutions. Thinning of a thick MoS_2 flake in (a–c) ethanol, (d–f) BMIM-PF6, and (g–i) DI water. Panels (a,d,g) show the optical images of the flake before laser scanning; panels (b,e,h) show the optical images of the flake after laser scanning; and panels (c,f,i) show the gate current during laser scanning.

degradation in PL intensity after laser excitation for 30 min (Figure S3, Supporting Information).

Exploring Mechanism of sOET. To fully understand the underlying mechanism of sOET, we conducted the thinning experiments in different solutions and monitored the current change during the thinning process. In non-conductive liquid (e.g., ethanol), the electrochemical reactions were inhibited (Figure 2a,b) since the optically activated electrons could not be extracted from MoS_2 to the electrode (the gate current is zero, Figure 2c). In an ion liquid (i.e., 1-butyl-3-methyl-imidazolium hexafluorophosphate, BMIM-PF6) with low electrical conductivity, a stable gate current of ~10 nA was observed (Figure 2f). However, the electrochemical thinning still did not happen (Figure 2d,e), which indicates the essential role of water (hydroxide ions) in the reaction. In contrast, with the existence of hydroxide ions, the MoS_2 flake was rapidly thinned in DI water (Figure 2g,h), which is weakly conductive to support the electron transfer. An increase in gate current was observed synchronously during the thinning process (Figure 2i), which indicates electron transfer during the thinning and proves that sOET is based on electrochemical reactions.

It should be noted that sOET preferably starts from the edge of TMD flakes with a high density of defects, while it cannot be initiated at the center region with limited detects. Defects at the flake edge could provide a large quantity of dangling bonds, which are important active sites for electrochemical reactions.[48] However, we could still initiate the laser thinning from the center of the flake via Ar^+ plasma treatment to increase the defect density. In addition, the photothermal effect in the sOET process is negligible. We experimentally measured the temperature of a MoS_2 flake in DI water under irradiation of a 785 nm laser using a phase camera (see the Methods section for more details). The temperature incease was not obvious under a typical operational power density (0.102 mW μm^{-2}) (Figure S4, Supporting Information). We also demonstrated successful thinning of TMD flakes on other conductive substrates, such as gold thin film and monolayer graphene, with the same configuration (Figure S5, Supporting Information). Interestingly, sOET could take place with no electrical bias on the gold film or graphene, which resulted from the spontaneous electron transfer from MoS_2 to the gold film or graphene,[49,50] similar to applying a bias voltage.

Tunable Thinning Rate of sOET. Based on the understanding of the thinning mechanisms, we achieved a

https://doi.org/10.1021/acsami.1c19163
ACS Appl. Mater. Interfaces 2021, 13, 58966–58973

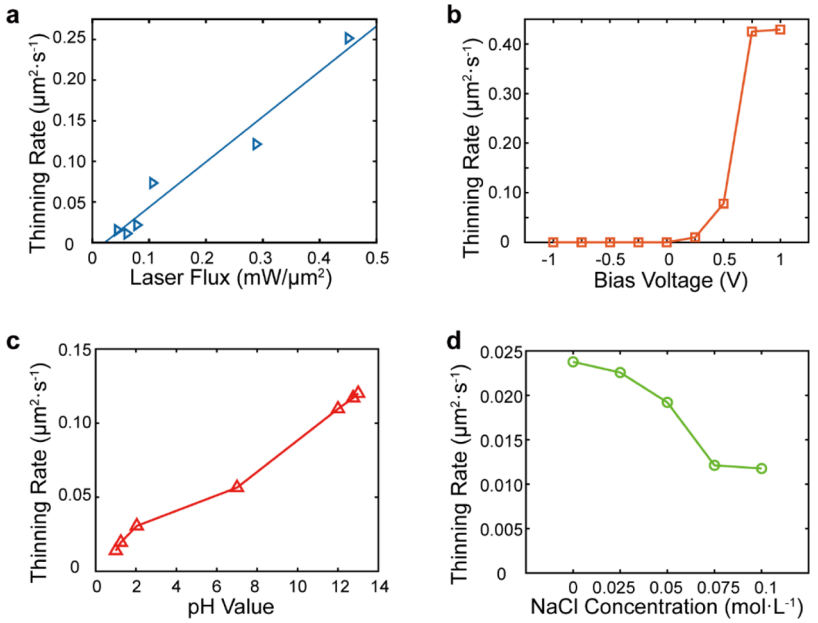

Figure 3. Tunable thinning rate of sOET. Thinning rate tuned by (a) laser power, (b) bias voltage, (c) pH value, and (d) NaCl concentration.

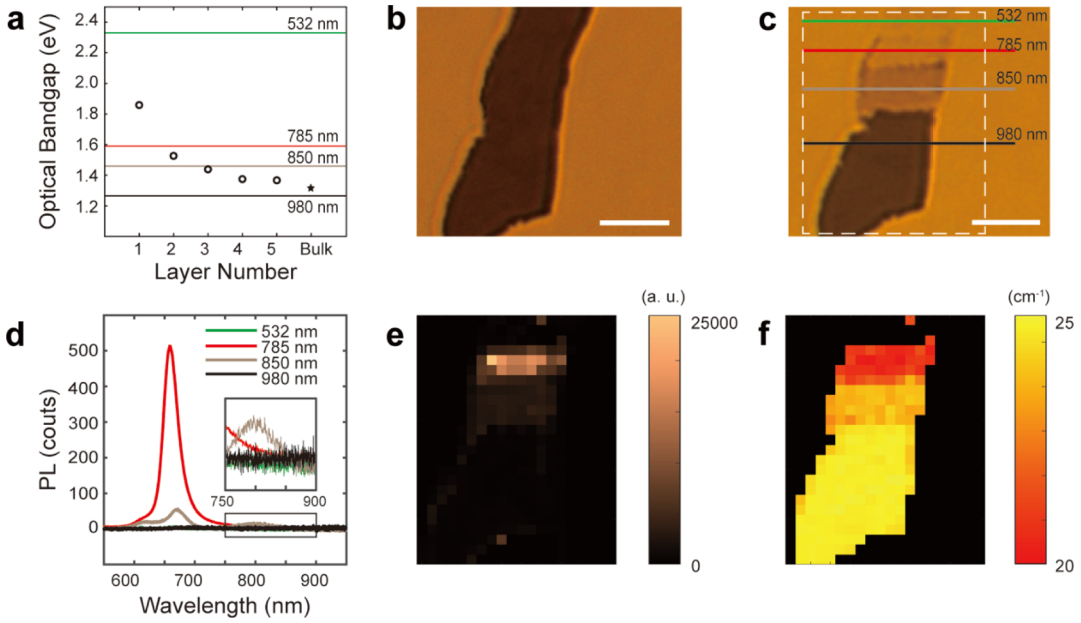

Figure 4. Thickness selectivity of sOET. (a) Working principle of thickness-selective thinning of MoS_2. By choosing excitation laser wavelength between these discrete layer-dependent band gaps, the thinning will stop once the band gap of the remaining layers is larger than the laser photon energy. (b) Thick MoS_2 flake before thinning. (c) Same flake in (b) after being thinned by 532, 785, 850, and 980 nm lasers at the specific sites. The laser-scanning paths are indicated by the green (532 nm), red (785 nm), gray (850 nm), and black (980 nm) lines. (d) PL spectra measured at the laser-scanned areas. (e) PL and (f) Raman mapping of the thinned regions [indicated by the white dashed rectangle in (c)]. All scale bars are 10 μm.

highly tunable thinning rate of sOET. First, since sOET is enabled by the optically activated electrochemical reactions, the thinning rate can be controlled by the laser power and the bias voltage. The thinning rate increased linearly along with the laser power (Figure 3a) as the optically excited electron density is proportional to the excitation power. Since sOET relies on the directional electron transfer, no obvious thinning was observed under a negative bias. When the bias increased from zero to positive, the thinning rate rose sharply and saturated at a bias of ~0.75 V (Figure 3b). The increase in the positive bias voltage can lead to more *p*-doping in TMD flakes and a faster electron transfer rate, which enhances the thinning rate. The saturation was ascribed to the limited optical pumping rate under a fixed laser power. In addition to the optical power and bias, the pH value and ionic concentration of solutions can remarkably affect the opto-electrochemical thinning. Figure 3c shows the thinning rate in sodium hydroxide/hydrochloride acid (NaOH/HCl) solutions with the same total ionic concentrations but different pH values (see the experimental section for details). Along with the increasing pH value, the concentration of hydroxide ions also increased, which provided more reactants in reaction eq 1 and enhanced the thinning

https://doi.org/10.1021/acsami.1c19163
ACS Appl. Mater. Interfaces 2021, 13, 58966−58973

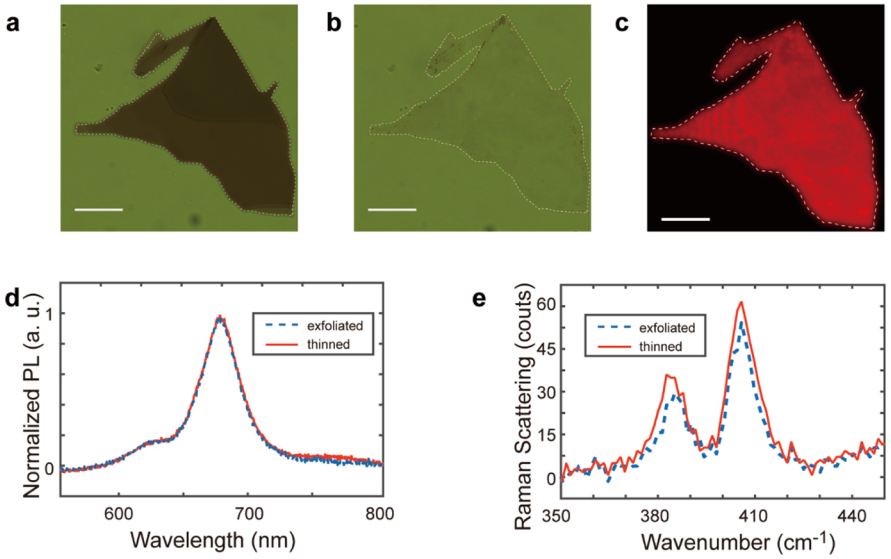

Figure 5. Mass production of high-quality monolayer TMDs via sOET. (a) Optical image of a large thick MoS_2 flake. (b) Optical image of the flake in (a) after being thinned by a 785 nm laser. (c) Fluorescence image of the thinned flake in (b). (d) Normalized PL and (e) Raman scattering spectra of the mechanically exfoliated and sOET thinned monolayer MoS_2. All the scale bars are 25 μm.

rate. In contrast, a higher concentration of other anions, such as Cl^-, could affect the thinning rate in a negative way (Figure 3d). This result is probably because nonreactive chloride ions can compete with reactive hydroxide ions to be attracted to the vicinity of the reactive sites.

Precise Thickness Control by sOET. Unlike the previously reported optoelectronic thinning methods that preferably thin bulk or few-layer TMDs to monolayers, sOET allows on-demand thinning of TMD flakes to the desired thickness. By selecting the laser photon energy according to the layer-dependent band gaps, sOET can realize the thinning of TMD flakes into different thicknesses. Taking MoS_2 as an example (Figure 4a), we show the thinning of a MoS_2 flake via sOET using 532, 785, 850, and 980 nm lasers. After thinning, the different thicknesses could be easily distinguished from the optical contrasts (Figure 4b,c), PL signals (Figure 4d,e), and Raman spectra (Figure 4f). A 980 nm laser (1.26 eV) cannot thin the MoS_2 flake since the photon energy is lower than the band gap of bulk MoS_2 (1.29 eV). In contrast, a 532 nm laser (2.33 eV) with the photon energy higher than the band gap of monolayer MoS_2 (1.84 eV) can remove all the flake as no PL or Raman signals were detected from the scanned area. Similarly, the use of a 785 nm or an 850 nm laser can lead to the thinning of a thick MoS_2 flake to a monolayer or bilayer. The PL and Raman measurements also showed the strongest PL intensity (Figure 4d) and smallest distance between two Raman modes (Figure S6, Supporting Information), which confirms the monolayer MoS_2 after thinning by a 785 nm laser. The bilayer MoS_2 thinned by an 850 nm laser was also proved by the indirect emission at ~805 nm (inset in Figure 4d).

Thinning of Large-Area TMDs by sOET. Last, we demonstrated the efficient thinning of large TMD flakes into the monolayer to show the potential of sOET in the mass production of the monolayer TMDs. A MoS_2 flake with the dimension of ~100 μm × 100 μm was successfully thinned into a monolayer by a 785 nm laser in less than 5 min (Figure 5a,b). The resultant monolayer showed strong and uniform PL under the excitation of a 532 nm laser (Figure 5c). The PL and Raman measurements showed comparable data with the mechanically exfoliated monolayer MoS_2 (Figure 5d,e), confirming the high quality of the thinned monolayers. It should be noted that the current thinning throughput is limited by our laser beam size and line-by-line scanning, which can be greatly improved with uniform large-area luminescence. In addition to MoS_2, our sOET also works for other TMD materials. For instance, the thinning of WSe_2 flakes into a monolayer was demonstrated by a 785 nm laser (Figure S7, Supporting Information), which proves the general applicability of sOET.

CONCLUSIONS

In summary, we have developed sOET for on-demand and high-throughput thinning of TMDs with excellent material quality. sOET is enabled by optically activated electrochemical reactions, where the thinning rate can be actively controlled by optical power, electrical bias, pH value, and ionic concentration. By rationally selecting laser photon energies based on the layer-dependent band gaps of TMD materials, we realized the precise control of the final thickness of the thinned TMD flakes. As a general technique, sOET is applicable to a wide range of TMD materials, which presents great potential for the mass production of high-quality TMD monolayers and few layers. With the low operational power, thickness-selective thinning, and site-specific patterning capabilities, sOET will provide new possibilities in the nanofabrication of TMD materials to advance their applications in many fields, including nanoelectronics and nanophotonics.

METHODS

Sample Preparation. ITO coverslips (SPI supplies) were cleaned by ultrasonication in acetone and isopropanol for 10 min, respectively, then rinsed by DI water and dried by nitrogen flow. TMD flakes were exfoliated from bulk materials to polydimethylsiloxane (PDMS) with the scotch tape. Then, the PDMS with TMD flakes was brought into contact with cleaned ITO coverslips and pressed for 10 min. Finally, the PDMS was removed by heating it up to 130 °C, and the TMD flakes were successfully transferred to the ITO coverslip. The samples

https://doi.org/10.1021/acsami.1c19163
ACS Appl. Mater. Interfaces 2021, 13, 58966−58973

were annealed under vacuum at 180 °C for 3 h to make good contacts between the TMD flakes and the ITO substrates.

sOET Procedure. The TMD flakes on ITO coverslips were mounted on an inverted microscope (Ti-E, Nikon). A solution (ethanol, DI water, NaCl solutions, or NaOH solutions) of ~200 μL volume was dropped on ITO to cover the TMD flakes. Electrical bias was applied using a Keithley SourceMeter (Keithley 2612B) with one electrode connecting the ITO and the other suspending in the solution. Lasers were directed to the TMDs from the bottom by a 40× objective (NA 0.75). The 532 nm (Ventus 532, Laser Quantum) and 785 nm (TEC 510, Sacher Lasertechnik) continuous-wave lasers were used. In addition, the 850 and 980 nm lasers were filtered by bandpass filters (Thorlabs) from a supercontinuum laser (SuperK FIANIUM-15, NKT photonics). During scanning, the stage was controlled by LabView programs. For the pH-dependent thinning experiments, the solutions were prepared by mixing 0.1 M NaOH and 0.1 M HCl solutions. The pH values were tuned by changing the ratio of NaOH and HCl and measured using a pH-meter. For the WSe_2 thinning experiments, 0.1 M NaOH solution was used. For other thinning experiments, DI water was used. After the thinning, the sample was rinsed by DI water for 15 s and dried by nitrogen flow to minimize the contaminants.

Optical Characterization. PL and Raman spectra were measured by a spectrometer (Andor) with an EMCCD (Andor). The signals were excited by a 532 nm laser and collected from a 100× objective (NA 0.6, Nikon). The laser power was set to be 250 μW for PL measurements and 755 μW for Raman measurements.

AFM Measurement. AFM measurement was carried out on a Park NX10 AFM (Park). The scanned area was set to be 60 nm × 60 nm. The scanning rate was 128 Hz. After measurement, the data were processed by Park XEI AFM data analysis software.

■ ASSOCIATED CONTENT

Supporting Information

The Supporting Information is available free of charge at https://pubs.acs.org/doi/10.1021/acsami.1c19163.

Setup illustration, additional results from PL, Raman mapping and temperature measurements, thinning on gold and graphene, and thinning of WSe_2 (PDF)

■ AUTHOR INFORMATION

Corresponding Authors

Xuezeng Zhao − *Key Laboratory of Micro-Systems and Micro-Structures Manufacturing of Ministry of Education and School of Mechatronics Engineering, Harbin Institute of Technology, Harbin 15001, China*; Email: zhaoxz@hit.edu.cn

Yuebing Zheng − *Walker Department of Mechanical Engineering, Material Science and Engineering Program and Texas Material Institute, The University of Texas at Austin, Austin, Texas 78712, United States*; orcid.org/0000-0002-9168-9477; Email: zheng@austin.utexas.edu

Authors

Suichu Huang − *Key Laboratory of Micro-Systems and Micro-Structures Manufacturing of Ministry of Education and School of Mechatronics Engineering, Harbin Institute of Technology, Harbin 15001, China; Walker Department of Mechanical Engineering, Material Science and Engineering Program and Texas Material Institute, The University of Texas at Austin, Austin, Texas 78712, United States*; orcid.org/0000-0001-5057-8095

Jingang Li − *Walker Department of Mechanical Engineering, Material Science and Engineering Program and Texas Material Institute, The University of Texas at Austin, Austin, Texas 78712, United States*; orcid.org/0000-0003-0827-9758

Jie Fang − *Walker Department of Mechanical Engineering, Material Science and Engineering Program and Texas Material Institute, The University of Texas at Austin, Austin, Texas 78712, United States*; orcid.org/0000-0002-0793-9323

Hongru Ding − *Walker Department of Mechanical Engineering, Material Science and Engineering Program and Texas Material Institute, The University of Texas at Austin, Austin, Texas 78712, United States*; orcid.org/0000-0003-1579-6825

Wentao Huang − *Key Laboratory of Micro-Systems and Micro-Structures Manufacturing of Ministry of Education and School of Mechatronics Engineering, Harbin Institute of Technology, Harbin 15001, China*

Complete contact information is available at: https://pubs.acs.org/10.1021/acsami.1c19163

Author Contributions

S.H. developed the initial idea and conducted all thinning experiments; J.L. worked on the AFM measurements and revised the manuscript; J.F. helped with the optical characterizations; H.D. helped with the temperature measurements. W.H., X.Z., and Y.Z. supervised this project. The manuscript was written through contributions of all authors. All authors have given approval to the final version of the manuscript.

Notes

The authors declare no competing financial interest.

■ ACKNOWLEDGMENTS

Y.Z. acknowledges the financial support of the National Science Foundation (NSF-ECCS-2001650). S.H. acknowledges the financial support of the China Scholarship Council (CSC no. 201906120139).

■ ABBREVIATIONS

2D, two-dimensional
AFM, atomic force microscopy
BMIM-PF6, 1-butyl-3-methylimidazolium hexafluorophosphate
CVD, chemical vapor deposition
DI, deionized
ITO, indium tin oxide
MBE, molecular beam epitaxy
PDMS, polydimethylsiloxane
PL, photoluminescence
sOET, self-limiting opto-electrochemical thinning
TMDs, transition-metal dichalcogenides

■ REFERENCES

(1) Novoselov, K. S.; Geim, A. K.; Morozov, S. V.; Jiang, D.; Zhang, Y.; Dubonos, S. V.; Grigorieva, I. V.; Firsov, A. A. Electric Field Effect in Atomically Thin Carbon Films. *Science* **2004**, *306*, 666−669.

(2) Choi, W.; Choudhary, N.; Akinwande, D.; Lee, Y. H.; Han, G. H.; Park, J. Recent Development of Two-Dimensional Transition Metal Dichalcogenides and Their Applications. *Mater. Today* **2017**, *20*, 116−130.

(3) Wang, Q. H.; Kalantar-Zadeh, K.; Kis, A.; Coleman, J. N.; Strano, M. S. Electronics and Optoelectronics of Two-Dimensional Transition Metal Dichalcogenides. *Nat. Nanotechnol.* **2012**, *7*, 699−712.

(4) Kalantar-zadeh, K.; Ou, J. Z.; Daeneke, T.; Strano, M. S.; Pumera, M.; Gras, S. L. Two-Dimensional Transition Metal Dichalcogenides in Biosystems. *Adv. Funct. Mater.* **2015**, *25*, 5086−5099.
(5) Manzeli, S.; Ovchinnikov, D.; Pasquier, D.; Yazyev, O. V.; Kis, A. 2D Transition Metal Dichalcogenides. *Nat. Rev. Mater.* **2017**, *2*, 17033.
(6) Wang, M.; Wu, Z.; Krasnok, A.; Zhang, T.; Liu, M.; Liu, H.; Scarabelli, L.; Fang, J.; Liz-Marzán, L. M.; Terrones, M.; Alù, A.; Zheng, Y. Dark-Exciton-Mediated Fano Resonance from a Single Gold Nanostructure on Monolayer WS2 at Room Temperature. *Small* **2019**, *15*, 1900982.
(7) Wang, M.; Krasnok, A.; Zhang, T.; Scarabelli, L.; Liu, H.; Wu, Z.; Liz-Marzán, L. M.; Terrones, M.; Alù, A.; Zheng, Y. Tunable Fano Resonance and Plasmon−Exciton Coupling in Single Au Nanotriangles on Monolayer WS2 at Room Temperature. *Adv. Mater.* **2018**, *30*, 1705779.
(8) Fang, J.; Wang, M.; Yao, K.; Zhang, T.; Krasnok, A.; Jiang, T.; Choi, J.; Kahn, E.; Korgel, B. A.; Terrones, M.; Li, X.; Alù, A.; Zheng, Y. Directional Modulation of Exciton Emission Using Single Dielectric Nanospheres. *Adv. Mater.* **2021**, *33*, 2007236.
(9) Mak, K. F.; Shan, J. Photonics and Optoelectronics of 2D Semiconductor Transition Metal Dichalcogenides. *Nat. Photonics* **2016**, *10*, 216−226.
(10) Zhang, Y.; Yao, Y.; Sendeku, M. G.; Yin, L.; Zhan, X.; Wang, F.; Wang, Z.; He, J. Recent Progress in CVD Growth of 2D Transition Metal Dichalcogenides and Related Heterostructures. *Adv. Mater.* **2019**, *31*, 1901694.
(11) Roch, J. G.; Froehlicher, G.; Leisgang, N.; Makk, P.; Watanabe, K.; Taniguchi, T.; Warburton, R. J. Spin-Polarized Electrons in Monolayer MoS 2. *Nat. Nanotechnol.* **2019**, *14*, 432−436.
(12) Novoselov, K. S.; Fal'ko, V. I.; Colombo, L.; Gellert, P. R.; Schwab, M. G.; Kim, K. A Roadmap for Graphene. *Nature* **2012**, *490*, 192−200.
(13) Peimyoo, N.; Deilmann, T.; Withers, F.; Escolar, J.; Nutting, D.; Taniguchi, T.; Watanabe, K.; Taghizadeh, A.; Craciun, M. F.; Thygesen, K. S.; Russo, S. Electrical Tuning of Optically Active Interlayer Excitons in Bilayer MoS2. *Nat. Nanotechnol.* **2021**, *16*, 888−893.
(14) Leisgang, N.; Shree, S.; Paradisanos, I.; Sponfeldner, L.; Robert, C.; Lagarde, D.; Balocchi, A.; Watanabe, K.; Taniguchi, T.; Marie, X.; Warburton, R. J.; Gerber, I. C.; Urbaszek, B. Giant Stark Splitting of an Exciton in Bilayer MoS2. *Nat. Nanotechnol.* **2020**, *15*, 901−907.
(15) Lee, J.-H.; Park, J. Y.; Cho, E. B.; Kim, T. Y.; Han, S. A.; Kim, T. H.; Liu, Y.; Kim, S. K.; Roh, C. J.; Yoon, H. J.; Ryu, H.; Seung, W.; Lee, J. S.; Lee, J.; Kim, S. W. Reliable Piezoelectricity in Bilayer WSe2 for Piezoelectric Nanogenerators. *Adv. Mater.* **2017**, *29*, 1606667.
(16) Liu, C. X. Unconventional Superconductivity in Bilayer Transition Metal Dichalcogenides. *Phys. Rev. Lett.* **2017**, *118*, 087001.
(17) Kanasugi, S.; Yanase, Y. Multiple Odd-Parity Superconducting Phases in Bilayer Transition Metal Dichalcogenides. *Phys. Rev. B* **2020**, *102*, 94507.
(18) He, Y.-M.; Clark, G.; Schaibley, J. R.; He, Y.; Chen, M.-C.; Wei, Y.-J.; Ding, X.; Zhang, Q.; Yao, W.; Xu, X.; Lu, C.-Y.; Pan, J.-W. Single Quantum Emitters in Monolayer Semiconductors. *Nat. Nanotechnol.* **2015**, *10*, 497−502.
(19) Chen, J.; Wang, Q.; Sheng, Y.; Cao, G.; Yang, P.; Shan, Y.; Liao, F.; Muhammad, Z.; Bao, W.; Hu, L.; Liu, R.; Cong, C.; Qiu, Z.-J. High-Performance WSe2 Photodetector Based on a Laser-Induced p-n Junction. *ACS Appl. Mater. Interfaces* **2019**, *11*, 43330−43336.
(20) Chen, Y.; Wang, Y.; Wang, Z.; Gu, Y.; Ye, Y.; Chai, X.; Ye, J.; Chen, Y.; Xie, R.; Zhou, Y.; Hu, Z.; Li, Q.; Zhang, L.; Wang, F.; Wang, P.; Miao, J.; Wang, J.; Chen, X.; Lu, W.; Zhou, P.; Hu, W. Unipolar Barrier Photodetectors Based on van Der Waals Heterostructures. *Nat. Electron* **2021**, *4*, 357−363.
(21) Schaibley, J. R.; Yu, H.; Clark, G.; Rivera, P.; Ross, J. S.; Seyler, K. L.; Yao, W.; Xu, X. Valleytronics in 2D Materials. *Nat. Rev. Mater.* **2016**, *1*, 16055.
(22) Li, L.; Shao, L.; Liu, X.; Gao, A.; Wang, H.; Zheng, B.; Hou, G.; Shehzad, K.; Yu, L.; Miao, F.; Shi, Y.; Xu, Y.; Wang, X. Room-Temperature Valleytronic Transistor. *Nat. Nanotechnol.* **2020**, *15*, 743−749.
(23) Hu, Y.; Huang, Y.; Tan, C.; Zhang, X.; Lu, Q.; Sindoro, M.; Huang, X.; Huang, W.; Wang, L.; Zhang, H. Two-Dimensional Transition Metal Dichalcogenide Nanomaterials for Biosensing Applications. *Mater. Chem. Front.* **2017**, *1*, 24−36.
(24) Ping, J.; Fan, Z.; Sindoro, M.; Ying, Y.; Zhang, H. Recent Advances in Sensing Applications of Two-Dimensional Transition Metal Dichalcogenide Nanosheets and Their Composites. *Adv. Funct. Mater.* **2017**, *27*, 1605817.
(25) Zhou, X.; Sun, H.; Bai, X. Two-Dimensional Transition Metal Dichalcogenides: Synthesis, Biomedical Applications and Biosafety Evaluation. *Front. Bioeng. Biotechnol.* **2020**, *8*, 236.
(26) Zhu, C.; Du, D.; Lin, Y. Graphene and Graphene-like 2D Materials for Optical Biosensing and Bioimaging: A Review. *2D Mater.* **2015**, *2*, 032004.
(27) Li, B. L.; Setyawati, M. I.; Chen, L.; Xie, J.; Ariga, K.; Lim, C.-T.; Garaj, S.; Leong, D. T. Directing Assembly and Disassembly of 2D MoS2 Nanosheets with DNA for Drug Delivery. *ACS Appl. Mater. Interfaces* **2017**, *9*, 15286−15296.
(28) Wang, S.; Chen, Y.; Li, X.; Gao, W.; Zhang, L.; Liu, J.; Zheng, Y.; Chen, H.; Shi, J. Injectable 2D MoS2-Integrated Drug Delivering Implant for Highly Efficient NIR-Triggered Synergistic Tumor Hyperthermia. *Adv. Mater.* **2015**, *27*, 7117−7122.
(29) Yadav, V.; Roy, S.; Singh, P.; Khan, Z.; Jaiswal, A. 2D MoS2-Based Nanomaterials for Therapeutic, Bioimaging, and Biosensing Applications. *Small* **2019**, *15*, No. e1803706.
(30) Huang, Y.; Pan, Y.-H.; Yang, R.; Bao, L.-H.; Meng, L.; Luo, H.-L.; Cai, Y.-Q.; Liu, G.-D.; Zhao, W.-J.; Zhou, Z.; Wu, L.-M.; Zhu, Z.-L.; Huang, M.; Liu, L.-W.; Liu, L.; Cheng, P.; Wu, K.-H.; Tian, S.-B.; Gu, C.-Z.; Shi, Y.-G.; Guo, Y.-F.; Cheng, Z. G.; Hu, J.-P.; Zhao, L.; Yang, G.-H.; Sutter, E.; Sutter, P.; Wang, Y.-L.; Ji, W.; Zhou, X.-J.; Gao, H.-J. Universal Mechanical Exfoliation of Large-Area 2D Crystals. *Nat. Commun.* **2020**, *11*, 2453.
(31) Huang, Y.; Sutter, E.; Shi, N. N.; Zheng, J.; Yang, T.; Englund, D.; Gao, H.-J.; Sutter, P. Reliable Exfoliation of Large-Area High-Quality Flakes of Graphene and Other Two-Dimensional Materials. *ACS Nano* **2015**, *9*, 10612−10620.
(32) Coleman, J. N.; Lotya, M.; O'Neill, A.; Bergin, S. D.; King, P. J.; Khan, U.; Young, K.; Gaucher, A.; De, S.; Smith, R. J.; Shvets, I. V.; Arora, S. K.; Stanton, G.; Kim, H.-Y.; Lee, K.; Kim, G. T.; Duesberg, G. S.; Hallam, T.; Boland, J. J.; Wang, J. J.; Donegan, J. F.; Grunlan, J. C.; Moriarty, G.; Shmeliov, A.; Nicholls, R. J.; Perkins, J. M.; Grieveson, E. M.; Theuwissen, K.; Mccomb, D. W.; Nellist, P. D.; Nicolosi, V. Two-Dimensional Nanosheets Produced by Liquid Exfoliation of Layered Materials. *Science* **2011**, *331*, 568−571.
(33) Backes, C.; Berner, N. C.; Chen, X.; Lafargue, P.; LaPlace, P.; Freeley, M.; Duesberg, G. S.; Coleman, J. N.; McDonald, A. R. Functionalization of Liquid-Exfoliated Two-Dimensional 2H-MoS2. *Angew. Chem., Int. Ed.* **2015**, *54*, 2638−2642.
(34) Amiri, A.; Naraghi, M.; Ahmadi, G.; Soleymaniha, M.; Shanbedi, M. A Review on Liquid-Phase Exfoliation for Scalable Production of Pure Graphene, Wrinkled, Crumpled and Functionalized Graphene and Challenges. *FlatChem* **2018**, *8*, 40−71.
(35) Lee, Y.-H.; Zhang, X.-Q.; Zhang, W.; Chang, M.-T.; Lin, C.-T.; Chang, K.-D.; Yu, Y.-C.; Wang, J. T.-W.; Chang, C.-S.; Li, L.-J.; Lin, T.-W. Synthesis of Large-Area MoS 2 Atomic Layers with Chemical Vapor Deposition. *Adv. Mater.* **2012**, *24*, 2320−2325.
(36) Roy, A.; Movva, H. C. P.; Satpati, B.; Kim, K.; Dey, R.; Rai, A.; Pramanik, T.; Guchhait, S.; Tutuc, E.; Banerjee, S. K. Structural and Electrical Properties of MoTe2 and MoSe2 Grown by Molecular Beam Epitaxy. *ACS Appl. Mater. Interfaces* **2016**, *8*, 7396−7402.
(37) Castellanos-Gomez, A.; Barkelid, M.; Goossens, A. M.; Calado, V. E.; Van Der Zant, H. S. J.; Steele, G. A. Laser-Thinning of MoS 2: On Demand Generation of a Single-Layer Semiconductor. *Nano Lett.* **2012**, *12*, 3187−3192.

https://doi.org/10.1021/acsami.1c19163
ACS Appl. Mater. Interfaces 2021, 13, 58966−58973

(38) Hu, L.; Shan, X.; Wu, Y.; Zhao, J.; Lu, X. Laser Thinning and Patterning of MoS2 with Layer-by-Layer Precision. *Sci. Rep.* **2017**, *7*, 15538.
(39) Cho, S.; Kim, S.; Kim, J. H.; Zhao, J.; Seok, J.; Keum, D. H.; Baik, J.; Choe, D.-H.; Chang, K. J.; Suenaga, K.; Kim, S. W.; Lee, Y. H.; Yang, H. Phase Patterning for Ohmic Homojunction Contact in MoTe2. *Science* **2015**, *349*, 625−628.
(40) Nagareddy, V. K.; Octon, T. J.; Townsend, N. J.; Russo, S.; Craciun, M. F.; Wright, C. D. Humidity-Controlled Ultralow Power Layer-by-Layer Thinning, Nanopatterning and Bandgap Engineering of MoTe2. *Adv. Funct. Mater.* **2018**, *28*, 1804434.
(41) Zhu, H.; Wang, Q.; Cheng, L.; Addou, R.; Kim, J.; Kim, M. J.; Wallace, R. M. Defects and Surface Structural Stability of MoTe2 under Vacuum Annealing. *ACS Nano* **2017**, *11*, 11005−11014.
(42) Rho, Y.; Pei, J.; Wang, L.; Su, Z.; Eliceiri, M.; Grigoropoulos, C. P. Site-Selective Atomic Layer Precision Thinning of MoS2 via Laser-Assisted Anisotropic Chemical Etching. *ACS Appl. Mater. Interfaces* **2019**, *11*, 39385−39393.
(43) Sunamura, K.; Page, T. R.; Yoshida, K.; Yano, T.-a.; Hayamizu, Y. Laser-Induced Electrochemical Thinning of MoS2. *J. Mater. Chem. C* **2016**, *4*, 3268−3273.
(44) Wu, S.-S.; Huang, T.-X.; Lin, K.-Q.; Yao, X.; Hu, J.-T.; Tang, D.-L.; Bao, Y.-F.; Ren, B. Photo-Induced Exfoliation of Monolayer Transition Metal Dichalcogenide Semiconductors. *2D Mater.* **2019**, *6*, 045052.
(45) Sakamaki, K. Photoelectrochemical in Situ Observation of N-MoS2 in Aqueous Solutions Using a Scanning Tunneling Microscope. *J. Vac. Sci. Technol., B: Microelectron. Nanometer Struct.–Process., Meas., Phenom.* **1991**, *9*, 944.
(46) Chakraborty, B.; Bera, A.; Muthu, D. V. S.; Bhowmick, S.; Waghmare, U. V.; Sood, A. K. Symmetry-Dependent Phonon Renormalization in Monolayer MoS 2 Transistor. *Phys. Rev. B: Condens. Matter Mater. Phys.* **2012**, *85*, No. 161403(R).
(47) Panasci, S. E.; Schilirò, E.; Greco, G.; Cannas, M.; Gelardi, F. M.; Agnello, S.; Roccaforte, F.; Giannazzo, F. Strain, Doping, and Electronic Transport of Large Area Monolayer MoS2Exfoliated on Gold and Transferred to an Insulating Substrate. *ACS Appl. Mater. Interfaces* **2021**, *13*, 31248−31259.
(48) Sivaram, S. V.; Hanbicki, A. T.; Rosenberger, M. R.; Jernigan, G. G.; Chuang, H.-J.; McCreary, K. M.; Jonker, B. T. Spatially Selective Enhancement of Photoluminescence in MoS 2 by Exciton-Mediated Adsorption and Defect Passivation. *ACS Appl. Mater. Interfaces* **2019**, *11*, 16147−16155.
(49) Lorchat, E.; López, L. E. P.; Robert, C.; Lagarde, D.; Froehlicher, G.; Taniguchi, T.; Watanabe, K.; Marie, X.; Berciaud, S. Filtering the Photoluminescence Spectra of Atomically Thin Semiconductors with Graphene. *Nat. Nanotechnol.* **2020**, *15*, 283−288.
(50) Bhanu, U.; Islam, M. R.; Tetard, L.; Khondaker, S. I. Photoluminescence Quenching in Gold-MoS 2 Hybrid Nanoflakes. *Sci. Rep.* **2014**, *4*, 5575.

https://doi.org/10.1021/acsami.1c19163
ACS Appl. Mater. Interfaces 2021, 13, 58966−58973